Investigation of Surface Structures of Dispersed V_2O_5 on CeO_2-SiO_2, CeO_2-TiO_2, and CeO_2-ZrO_2 Mixed Oxides by XRD, Raman, and XPS Techniques

Benjaram M. Reddy,* Pandian Lakshmanan, and Ataullah Khan

Inorganic and Physical Chemistry Division, Indian Institute of Chemical Technology, Hyderabad - 500 007, India

Received: June 26, 2004; In Final Form: August 18, 2004

The techniques of X-ray diffraction (XRD), Raman spectroscopy (RS), and X-ray photoelectron spectroscopy (XPS) were employed to investigate dispersion and structural characteristics of V_2O_5/CeO_2-MO_2 ($M = Si^{4+}$, Ti^{4+}, and Zr^{4+}) catalysts calcined at different temperatures from 773 to 1073 K. The CeO_2-MO_2 (1:1 mole ratio) mixed oxides were obtained by soft chemical methods with ultrahigh-dilution solutions, and a nominal monolayer equivalent of V_2O_5 was deposited over the calcined (773 K) supports. The XRD and RS results suggest that the CeO_2-MO_2 carrier calcined at 773 K exhibits the presence of nanocrystalline cubic CeO_2 on the surface of SiO_2 in CeO_2-SiO_2, CeO_2 and TiO_2 (anatase) in CeO_2-TiO_2, and $Ce_{0.75}Zr_{0.25}O_2$ in CeO_2-ZrO_2 samples. The impregnation of vanadia over CeO_2-MO_2 and their subsequent calcination at higher temperatures leads to various modifications. The deposited V_2O_5 is in a highly dispersed state when calcined at 773 K. In particular, no crystalline V_2O_5 is observed at all calcination temperatures. The dispersed vanadia on the CeO_2-MO_2 carrier induces better crystallization of various phases and a preferential formation of $CeVO_4$ in all samples. Incorporation of more zirconia into the $Ce_{0.75}Zr_{0.25}O_2$ cubic lattice leading to the manifestation of a $Ce_{0.16}Zr_{0.84}O_2$ tetragonal phase at higher calcination temperatures is noted in the case of CeO_2-ZrO_2 samples. The RS measurements disclose the presence of oxygen vacancies/Ce^{3+} in all samples in different proportions. The XPS results reveal that O 1s, Ce 3d, and V 2p core-level photoelectron peaks are sensitive to the calcination temperature and the nature of mixed-oxide system. The formation of $CeVO_4$ at various temperatures is established from all characterization results.

1. Introduction

Supported vanadium oxide catalysts are very complex inorganic materials that play an important role in heterogeneous catalysis in both the gas and liquid phases.[1−5] Reactions catalyzed by these oxides are numerous, including oxidative dehydrogenation of alkanes,[6,7] selective catalytic reduction of NO_x with NH_3,[8,9] partial oxidation of various hydrocarbons,[10,11] ammoxidation of substituted aromatic compounds,[12,13] and direct conversion of methane to aromatics.[14] Although unsupported vanadium pentoxide is active in most of the redox reactions, its selectivity to the desired products is low and mostly favors deep oxidation. Deposition of V_2O_5 on the surface of an appropriate oxide support (mostly Al_2O_3, SiO_2, and TiO_2) of high specific surface area improves the catalytic activity and selectivity of a number of reactions.[5] In particular, the nature of support plays a huge influence on the physicochemical and catalytic properties of the supported vanadium oxide catalysts. As a consequence, considerable attention has been devoted to the characterization of dispersed vanadium oxide on various supports.

Ceria-based materials have been receiving tremendous attention recently because of their diverse uses in catalysis and materials science. Significant applications of CeO_2-based materials include three-way catalysts (TWC),[15−17] fuel cell processes,[15,18] oxygen permeation membrane systems,[19] deNO_x catalysis,[20] exhaust combustion catalysts,[15,21,22] and catalytic wet oxidation.[15,23] The success of ceria in pollution abatement and other technologies is mainly due to its unique combination of elevated oxygen transport capacity coupled with the ability to shift easily between reduced and oxidized states ($Ce^{3+} \leftrightarrow Ce^{4+}$).[24] Mainly ceria-based noble metal catalysts are being employed for various catalytic applications because of their increased reactivity.[25−27] However, transition-metal oxide-based ceria catalysts may be an alternative, because these are much cheaper than noble metals, allowing a higher catalyst load, which can compensate for the reduced reactivity.

Recent investigations reveal that V_2O_5/CeO_2 combination catalysts exhibit good catalytic activity for oxidative conversion of propane to propylene and ethylene,[28,29] partial oxidation of methanol to formaldehyde,[30,31] preferential oxidation of CO to CO_2, and others.[32,33] It is quite obvious that the combination of vanadia (known for its redox properties) and ceria (known for its oxygen storage and release functions) can give rise to better catalytic systems. These catalysts are also expected to perform extraneous redox reactions for both selective and nonselective oxidations, the latter having extensive applications in the field of environmental catalysis for the oxidative removal of volatile organic compounds and other noxious emissions. However, a major disadvantage associated with CeO_2 support is its relatively low specific surface area and low thermal stability. Recent studies suggest that the formation of mixed oxides of ceria with cations such as Zr^{4+}, Al^{3+}, and La^{3+} enhances the thermal stability, redox, and oxygen storage properties of ceria.[24,34,35] Therefore, an effort has been made in the present investigation to understand the dispersion and nature of vanadium oxide on CeO_2-MO_2 ($M = Si^{4+}$, Ti^{4+}, and Zr^{4+}) mixed-oxide supports

* To whom correspondence should be addressed. Phone: +91-40-27160123. Fax: +91-40-27160921. E-mail: bmreddy@iict.res.in, mreddyb@yahoo.com.

10.1021/jp047217q CCC: $27.50
Published on Web 10/06/2004

under the influence of thermal treatments. Many groups have extensively investigated the surface structures of vanadia on various single and mixed-oxide supports in the literature.[4−6,36−40] However, studies on the dispersion of V_2O_5 exclusively over ceria-based mixed oxides have not been attempted, to the best of our knowledge. In this study, various CeO_2-MO_2 (1:1 mole ratio) mixed oxides obtained by soft chemical routes were impregnated with a monolayer equivalent of V_2O_5 and subjected to thermal treatments from 773 to 1073 K. The resulting catalysts were investigated by means of X-ray diffraction (XRD), Raman spectroscopy (RS), X-ray photoelectron spectroscopy (XPS), and other techniques.

2. Experimental Section

2.1. Preparation of Catalysts. The various CeO_2-MO_2 ($M = Si^{4+}$, Ti^{4+}, and Zr^{4+}) mixed-oxide supports (1:1 molar ratio based on oxides) employed in this study to impregnate with vanadium pentoxide were prepared by soft chemical methods using ultrahigh-dilution solutions. To prepare CeO_2-TiO_2, the desired quantities of $CeCl_3 \cdot 7H_2O$ (99.0%, Aldrich) and $TiCl_4$ (99.9%, Aldrich) were dissolved separately in excess double-distilled water and mixed together. To make CeO_2-ZrO_2, the requisite quantities of ammonium cerium(IV) nitrate (Loba Chemie, GR grade) and zirconium(IV) nitrate (Fluka, AR grade) were dissolved separately and mixed together. To obtain CeO_2-SiO_2, the requisite quantities of cerium ammonium nitrate (Loba Chemie, GR grade), dissolved separately in deionized water, and colloidal silica (40 wt %, Fluka, AR grade) were mixed together. Dilute aqueous ammonia was added dropwise gradually to the aforementioned mixture solutions with vigorous stirring, until precipitation was complete (pH = 8). The obtained hydroxide gels were thoroughly washed until free from anionic impurities, oven dried at 393 K for 12 h, and calcined at 773 K for 5 h in air atmosphere. A monolayer equivalent of V_2O_5 was deposited over the calcined supports (773 K) by a wet impregnation method.[5] To achieve this, requisite quantities of NH_4VO_3 (Fluka, AR grade) were dissolved in 0.2 M aqueous oxalic acid (Loba Chemie, GR grade) solution, and to this solution, finely powdered (calcined at 773 K) supports were added. The excess water was evaporated in a water bath under constant stirring. The obtained materials were oven-dried at 393 K for 12 h and subsequently calcined at 773 K for 5 h in flowing oxygen. Small portions of the calcined catalysts were once again heated at 873, 973, and 1073 K for 5 h. The rate of heating, as well as cooling, was always maintained at 5 K/min.

2.2. Characterization of Samples. XRD patterns of the powdered samples were recorded on a Siemens D-500 diffractometer using a nickel-filtered Cu Kα (0.15418 nm) radiation source. The intensity data were collected over a 2θ range of 3−80° with a 0.02° step size and using a counting time of 1 s per point. Various crystalline phases present in the samples were identified with the reference data from International Centre for Diffraction Data (ICDD) files. The average crystallite sizes of CeO_2 and $Ce_{0.75}Zr_{0.25}O_2$ were estimated with the help of the Debye−Scherrer equation using the XRD data of all prominent lines.[41]

The Raman spectra were recorded on a DILOR XY spectrometer equipped with a liquid-nitrogen-cooled charge-coupled device (CCD) detector. The emission line at 514.5 nm from the Ar^+ ion laser (Spectra Physics) was focused on the sample under the microscope, with the width of the analyzed spot being ~1 μm. The power of the incident beam on the sample was 3 mW. The time of acquisition was adjusted according to the intensity of the Raman scattering. The wavenumber values reported from the spectra are accurate to within 2 cm^{-1}. For each sample, the spectra were recorded at several points in order to ascertain the homogeneity of the sample, and the average of all these spectra were plotted in the figures presented in this study.

TABLE 1: BET Surface Area and Crystallite Size Measurements in Various V_2O_5/CeO_2-MO_2 ($M = Si^{4+}$, Ti^{4+}, and Zr^{4+}) Samples Calcined at Different Temperatures

sample/ calcination temperature (K)	surface area ($m^2\ g^{-1}$)	crystallite size (nm)
CeO_2-SiO_2 (773 K)	147	3.2[a]
10 wt % V_2O_5/CeO_2-SiO_2		
773	78	3.8[a]
873	40	7.6[a]
973	32	13.9[a]
1073	17	20.6[a]
CeO_2-TiO_2 (773 K)	59	10.0[a]
5 wt % V_2O_5/CeO_2-TiO_2		
773	44	12.9[a]
873	38	14.6[a]
973	29	16.8[a]
1073	14	22.3[a]
CeO_2-ZrO_2 (773 K)	84	4.7[b]
12 wt % V_2O_5/CeO_2-ZrO_2		
773	66	5.0[b]
873	27	5.6[b]
973	20	5.7[b]
1073	18	6.0[b]

[a] CeO_2. [b] $Ce_{0.75}Zr_{0.25}O_2$.

The XPS measurements were performed on a Shimadzu (ESCA 3400) spectrometer by using Mg Kα (1253.6 eV) radiation as the excitation source. The charging of catalyst samples was corrected by setting the binding energy of the adventitious carbon (C 1s) at 284.6 eV.[42,43] The XPS analysis was done at ambient temperature and pressures typically on the order of less than 10^{-6} Pa. Prior to analysis, the samples were outgassed in a vacuum oven overnight. Quantification of the atomic ratios was achieved by determining the elemental peak areas, following a Shirley background subtraction by the usual procedures documented in the literature.[42,43]

The BET surface areas were determined by N_2 physisorption at liquid N_2 temperature on a Micromeritics Gemini 2360 instrument. Prior to analysis, the samples were oven-dried at 393 K for 12 h and flushed with Argon gas for 2 h.

3. Results and Discussion

The N_2 BET surface areas of various supports calcined at 773 K and V_2O_5-containing catalysts calcined from 773 to 1073 K are presented in Table 1. All of the mixed-oxide supports investigated exhibit reasonably high surface area (SA). Upon impregnation of the supports with V_2O_5, a substantial loss in the BET SA could be noted. This is a general phenomenon observed in the case of supported catalysts when an active component is impregnated over its surface.[5] The observed decrease is mainly due to penetration of the dispersed vanadium oxide into the pores of the support, thereby narrowing its pore diameter and blocking some of the micropores.[5,36] The subsequent decline in the surface areas upon thermal treatments at higher temperatures could be attributed to particle growth (sintering) and preferential solid-state interactions between the dispersed vanadium oxide and the supporting oxides.[44,45] The XRD and RS measurements described in the subsequent paragraphs strongly support the latter possibility.

The XRD patterns of V_2O_5/CeO_2-SiO_2, V_2O_5/CeO_2-TiO_2, and V_2O_5/CeO_2-ZrO_2 samples calcined at various temperatures

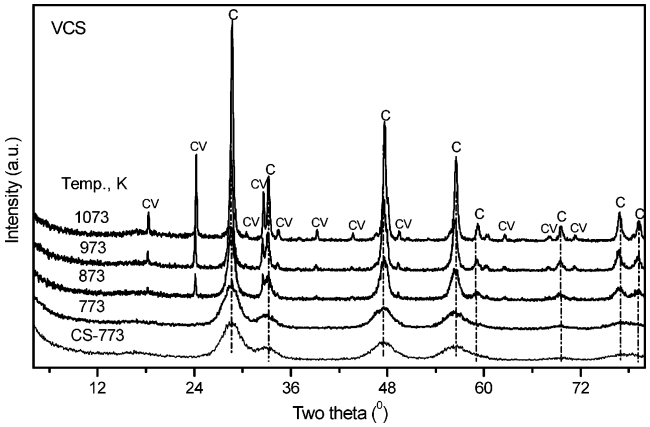

Figure 1. Powder X-ray diffraction (XRD) patterns of 10 wt % V_2O_5/CeO_2-SiO_2 catalysts calcined at different temperatures. Peak legend is as follows: C, lines due to CeO_2; CV, lines due to $CeVO_4$.

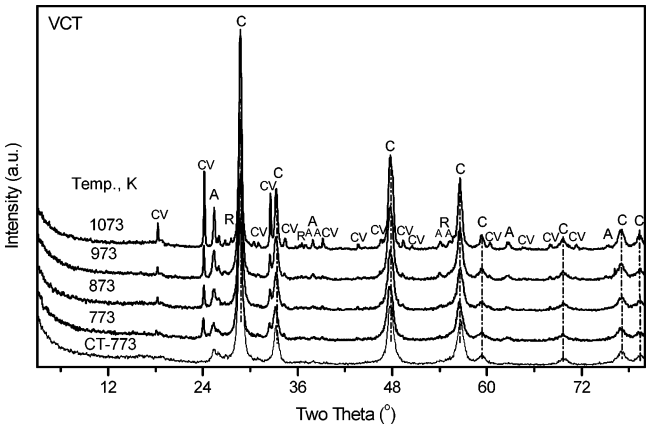

Figure 2. Powder X-ray diffraction (XRD) patterns of 5 wt % V_2O_5/CeO_2-TiO_2 catalysts calcined at different temperatures. Peak legend is as follows: C, lines due to CeO_2; A, lines due to TiO_2−anatase; R, lines due to TiO_2−rutile; CV, lines due to $CeVO_4$.

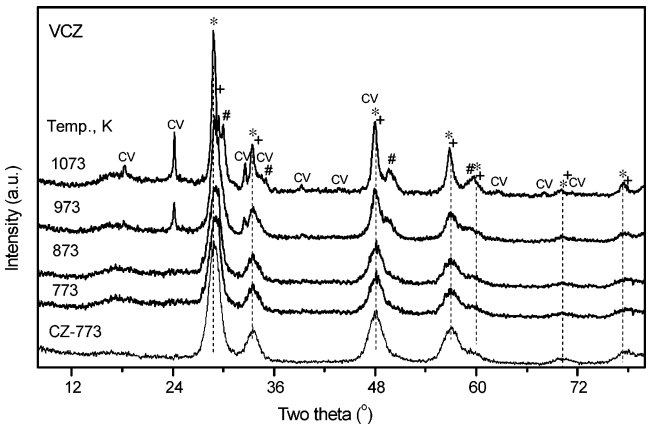

Figure 3. Powder X-ray diffraction (XRD) patterns of 12 wt % V_2O_5/CeO_2-ZrO_2 catalysts calcined at different temperatures. Peak legend is as follows: (*), lines due to $Ce_{0.75}Zr_{0.25}O_2$; (+), lines due to $Ce_{0.6}Zr_{0.4}O_2$; (#), lines due to $Ce_{0.16}Zr_{0.84}O_2$; CV, lines due to $CeVO_4$.

from 773 to 1073 K are presented in Figures 1−3, respectively. The corresponding XRD patterns of the supports calcined at 773 K are also shown in these figures. As shown in Figure 1, the CeO_2-SiO_2 sample calcined at 773 K exhibits poor crystallinity. Only the broad diffraction lines pertaining to cubic CeO_2 (PDF-ICDD 34-0394) could be seen. The characteristic lines due to SiO_2 are absent, indicating that it is in an amorphous state. Also, the absence of crystalline features of V_2O_5 in the case of the V_2O_5/CeO_2-SiO_2 sample calcined at 773 K indicate that vanadium oxide is in a highly dispersed or amorphous form on the surface of the support. However, at 873 K in addition to the sharp CeO_2 lines, some new lines with less intensity could be seen at $2\theta = 18.5$, 24, and 32.5, respectively. These lines are due to the formation of crystalline $CeVO_4$ (PDF-ICDD 12-0757) compound. The intensity of these lines increased with increasing calcination temperature. However, no XRD lines due to crystalline SiO_2 or compounds of it with CeO_2 or V_2O_5 are noted even at 1073 K. Recently, Rocchini et al.[46,47] reported the formation of an intermediate $Ce_{9.33}(SiO_4)_6O_2$ phase between CeO_2 and SiO_2, which, on suitable treatment, decomposed into amorphous silica and smaller crystallites of ceria. This intermediate phase was attributed to the enhanced textural and thermal stability of CeO_2-SiO_2 mixed oxides. The absence of this compound in the present study could be due to a different preparation method adopted and lower calcination temperatures employed.

As presented in Figure 2, the XRD patterns of the CeO_2-TiO_2 sample calcined at 773 K provide typical diffraction patterns of the cubic CeO_2 along with less intense peaks due to TiO_2−anatase phase (PDF-ICDD 21-1272). In the case of the V_2O_5/CeO_2-TiO_2 sample calcined at 773 K, along with the prominent CeO_2 and TiO_2 (A) lines, a few new diffraction peaks due to the formation of the $CeVO_4$ compound could be observed. The intensity of all these lines increased with increasing calcination temperature. Interestingly, no characteristic diffraction lines due to crystalline V_2O_5 are noted. A few new lines with less intensity are observed at 1073 K, which could be assigned to TiO_2 rutile phase (PDF-ICDD 21-1276). The formation of various crystalline compounds, namely, Ce_2TiO_5, $Ce_2Ti_2O_7$, and $Ce_4Ti_9O_{24}$, were reported in the literature between Ce−Ti oxides when heated at 1523 K.[48] No such crystalline phases are observed in the present study, presumably because of a different preparation method adopted and lower calcination temperatures employed.

As shown in Figure 3, the XRD patterns of the CeO_2-ZrO_2 sample calcined at 773 K indicate only the broad diffraction lines due to a cubic fluorite-type phase with the composition $Ce_{0.75}Zr_{0.25}O_2$ (PDF-ICDD 28-0271). The XRD patterns pertaining to the same phase are also visible in the case of the V_2O_5/CeO_2-ZrO_2 sample calcined at 773 K. However, with an increase in calcination temperature from 773 to 1073 K, the emergence of additional new lines pertaining to another cubic fluorite-type phase with the composition $Ce_{0.4}Zr_{0.6}O_2$ (PDF-ICDD 38-1439) and a tetragonal phase with the composition $Ce_{0.16}Zr_{0.84}O_2$ (PDF-ICDD 38-1437) are visible. The appearance of these phases at higher calcination temperatures indicates that a progressive increase of zirconia content in the ceria unit cell is taking place as a function of increasing calcination temperature. Interestingly, here again no XRD lines pertaining to crystalline V_2O_5 are observed. This gives an impression that the impregnated vanadium oxide is in a highly dispersed or amorphous state on the surface of the support. However, at 973 and 1073 K, the formation of $CeVO_4$ is clearly observed, as in earlier cases. The preferential formation of $CeVO_4$ in V_2O_5/CeO_2-MO_2 ($M = Si^{4+}$, Ti^{4+}, and Zr^{4+}) systems gives an impression that vanadium oxide selectively interacts with the ceria portion of these mixed oxides and forms this stable compound. However, its formation temperature is varied from system to system.

Crystallite size (D_{XRD}) of CeO_2 in V_2O_5/CeO_2-SiO_2 and V_2O_5/CeO_2-TiO_2 samples, and $Ce_{0.75}Zr_{0.25}O_2$ in V_2O_5/CeO_2-ZrO_2, as a function of calcination temperature, is summarized

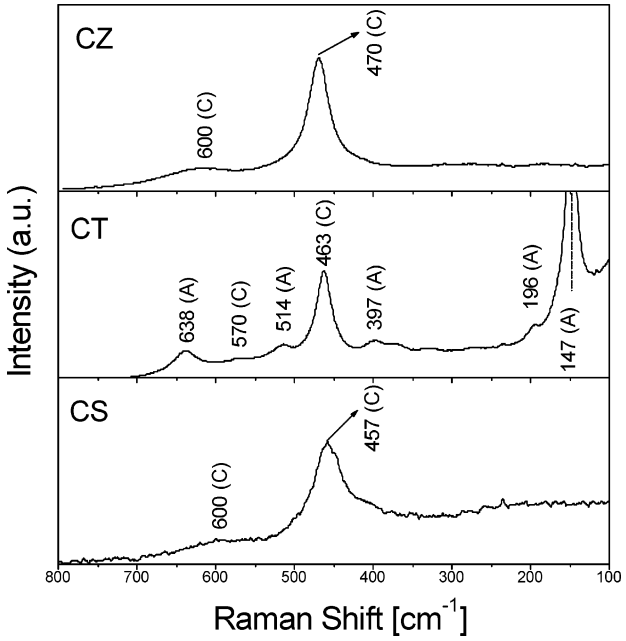

Figure 4. Raman spectra of various CeO_2-MO_2 (M = Si^{4+}, Ti^{4+}, and Zr^{4+}) samples calcined at 773 K.

in Table 1. As can be noted from this table, an increase in the crystallite size is observed in all samples with increasing calcination temperature, and the increase is meager in the case of V_2O_5/CeO_2-ZrO_2 samples. When compared to pure supports, the crystallite size in V_2O_5-containing catalysts is larger, which indicates that the impregnated vanadium oxide accelerates the grain growth of CeO_2 and $Ce_{0.75}Zr_{0.25}O_2$ in various samples. Thus, it can be inferred from Table 1 that the crystallization depends both on the calcination temperature as well as on the presence of dispersed vanadium oxide. Interestingly, the XRD measurements in the case of V_2O_5/CeO_2-ZrO_2 samples indicate that impregnated vanadium oxide not only accelerates the grain growth of ceria−zirconia solid solutions but also induces more incorporation of zirconia into the ceria cubic lattice, leading to the formation of a zirconia-rich tetragonal phase.[49]

Raman spectroscopy is a promising technique for the elucidation of structures of complex transition-metal oxides present either as bulk phases or as two-dimensional supported phases. In particular, RS directly probes structures and bonds by its vibrational spectrum. Therefore, this technique has been extensively used to discriminate between different structures on oxide surfaces.[50] Raman spectra of all the support oxides calcined at 773 K are shown in Figure 4. In general, the Raman spectrum of CeO_2 is characterized by a strong band at 462 cm^{-1} due to the F_{2g} Raman active mode of the fluorite structure.[51] In addition, it also exhibits a weak band at ∼260 cm^{-1} and a shoulder at ∼600 cm^{-1}, which have been attributed to the normal Raman inactive (IR active) transverse and longitudinal optical (LO) phonon modes, respectively, at the Brillouin zone center.[52] As shown in Figure 4, all samples show a prominent peak at 457−470 cm^{-1} and a weak band at ∼600 cm^{-1}. The band at 457 cm^{-1}, in the case of the CeO_2-SiO_2 sample, corresponds to the triply degenerate F_{2g} mode and can be viewed as a symmetric breathing mode of oxygen atoms around cerium ions.[53] The weak band observed near 600 cm^{-1} could correspond to a nondegenerate LO mode of CeO_2.[53−55] Normally, this mode should not be observed by Raman spectroscopy, but the presence of some defects can involve the relaxation of selection rules. In particular, this band has been linked to oxygen vacancies in the CeO_2 lattice.[56] This band was observed in the case of nanosized samples, and its relative intensity increased as the particle size got smaller.[53] The same phenomenon is apparent in the present study, too. For each sample, the spectra were recorded at several points, and no shift in the band position or difference of width was noted. This observation reveals clearly that all of the samples are mostly in a homogeneous state. Silica did not show any Raman features, as reported in the literature.[57] This gives an impression that silica forms part of the substrate support on which ceria has been forming a surface overlayer. The absence of any other Raman features provides one more inference that silica is not forming any compound with cerium oxide, in line with XRD observations. The Raman spectra of the CeO_2-TiO_2 sample reveals a typical spectra of TiO_2−anatase (space group I_1/amd) and CeO_2.[53] The Raman bands pertaining to the anatase phase appear at 147, 196, 397, 514, and 638 cm^{-1}.[53] In agreement with XRD measurements, there is again no evidence about the formation of detectable compounds between ceria and titania from the Raman results. The Raman spectrum of CeO_2-ZrO_2 sample calcined at 773 K is dominated by a strong band at ∼470 cm^{-1} and a less prominent, broad band at ∼600 cm^{-1}. The band at ∼470 cm^{-1} can be attributed to the F_{2g} vibration of the fluorite-type lattice. The slight shift in the Raman frequency to higher wavenumbers could be due to the incorporation of zirconium ions into the ceria lattice, as evidenced by XRD results. No Raman lines due to ZrO_2 could be observed, in line with XRD measurements. Thus, the Raman results corroborate well with the XRD observations.

The Raman spectra of various V_2O_5-impregnated samples, calcined at 773 and 1073 K and recorded in the range 100−1200 cm^{-1}, are shown in Figure 5. The spectrum of the V_2O_5/CeO_2-SiO_2 sample calcined at 773 K exhibits a prominent peak at ∼457 cm^{-1} and a few broad bands of low intensity at ∼600, ∼850, ∼700−900, and ∼1000 cm^{-1}. With increase of calcination temperature from 773 to 1073 K, sharpening of the band at 457 cm^{-1} with a slight shift toward higher wavenumbers (due to better crystallization) and diminishing of the other bands could be noted. Furthermore, some new bands were observed at ∼234, ∼261, ∼378, 785, 797, and 860 cm^{-1}.[58] These new bands are due to the formation of $CeVO_4$. No crystalline V_2O_5 features (Raman bands at ∼995, ∼702, ∼527, ∼404, ∼284, and ∼146 cm^{-1}) are observed, in agreement with XRD results. In general, the spectrum of the sample calcined at 773 K is characteristic of vanadia supported on a poorly crystalline CeO_2 support. However, the spectrum of the sample calcined at 1073 K is completely different, because it evidences mainly well-crystallized CeO_2 and $CeVO_4$. The Raman spectrum of the V_2O_5/CeO_2-TiO_2 sample calcined at 773 K exhibits prominent peaks due to titania−anatase and cubic ceria along with broad and less intense bands in the regions at ∼930 and 995−1020 cm^{-1}. With increasing calcination temperature, the intensity of the bands pertaining to both the anatase and ceria phases increased proportionately, while the broad bands at ∼930 and 995−1020 cm^{-1} disappeared progressively. At higher calcination temperatures, the new peaks pertaining to $CeVO_4$ phase could be seen.[50] According to literature reports, the TiO_2−rutile phase exhibits bands at 144, 148, and 611 cm^{-1}, whose presence could be seen at 1073 K.[59] No crystalline V_2O_5 features are apparent, in line with XRD observations. At a 773 K calcination temperature, the impregnated vanadia is mostly in a highly dispersed state on the surface of CeO_2-TiO_2. With increasing calcination temperature, the formation of $CeVO_4$ compound is observed at the expense of the dispersed vanadium oxide species. Similar findings were reported by Bañares and Wachs for

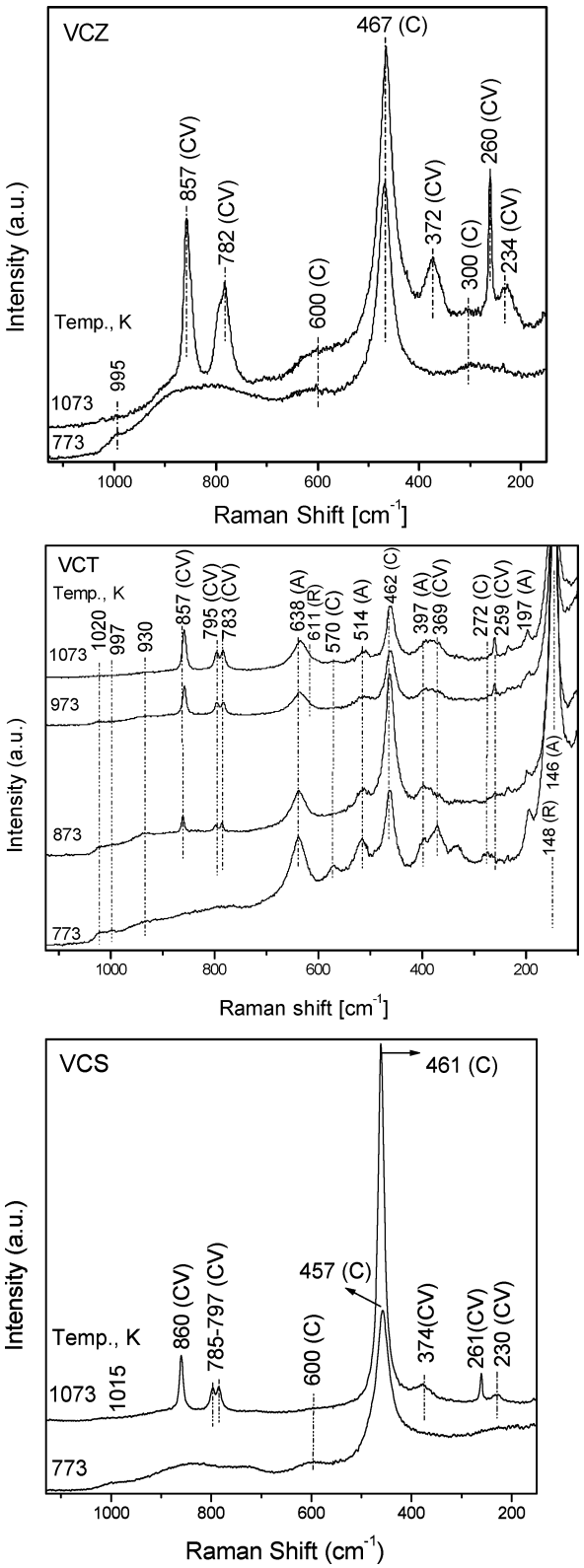

Figure 5. Raman spectra of various V_2O_5/CeO_2-MO_2 (M = Si^{4+}, Ti^{4+}, and Zr^{4+}) catalysts calcined at different temperatures.

dehydrated VO_x/CeO_2 catalysts.[50] The V_2O_5/CeO_2-ZrO_2 sample calcined at 773 K exhibits a prominent Raman peak at ~467 cm^{-1} (ceria cubic form) along with broad and less intense bands in the regions of ~210−320, ~600, ~700−900, and ~995 cm^{-1}. The broad band in the range 540−600 cm^{-1} could be assigned to a band that originates from the oxygen vacancies in the ceria lattice.[56] This is primarily due to partial reduction of the sample (Ce^{4+} into Ce^{3+}), which leads to the formation of additional oxygen vacancies to satisfy electrical neutrality. With increasing calcination temperature, sharpening of the band at ~467 cm^{-1} is observed, along with the appearance of new bands signifying the formation of the $CeVO_4$ compound.[50] Thus, the Raman results in corroboration with the XRD measurements demonstrate the formation of $CeVO_4$ in parallel with the disappearance of the dispersed vanadium oxide (both isolated as well as polymeric vanadium oxide species) and also a better crystallization of the cubic fluorite-type structure at higher calcination temperatures.

As per the literature reports, the tetrahedral VO_4^{3-}, present in aqueous solution, has the most prominent Raman band at 827 cm^{-1}, and for solids, with isolated VO_4^{3-} units, this band lies in the range 830−860 cm^{-1}.[60] This band is associated with the breathing mode of the tetrahedron. In $CeVO_4$, vanadium ions are placed at the centers of oxygen tetrahedra with a vanadium−oxygen distance (d_{V-O} = 1.7 Å) similar to that of an isolated VO_4^{3-}. Therefore, the band at 857−860 cm^{-1} of $CeVO_4$ could be assigned to such a mode. In general, the Raman bands of the supported metal oxide catalysts in the range between 1050 and 950 cm^{-1} can be assigned to the stretching mode of the short terminal M═O bonds, whereas the bands in the range 950−750 cm^{-1} are attributed to either the antisymmetric stretch of the M−O−M bonds or the symmetric stretch of the $(-O-M-O-)_n$ bonds.[50,61,62] The major peak of crystalline V_2O_5 assigned to the V═O stretching mode appears at ~995 cm^{-1}. Because of a relatively large Raman scattering cross-section of V_2O_5 as compared to the cross-section for supported vanadia species, the Raman spectra of supported vanadia catalysts can appear to be essentially similar to those of the bulk V_2O_5.[5] Therefore, the presence of a weak band at ~995 cm^{-1} in the case of the 773 K calcined samples can be assigned to the dispersed vanadium oxide on the surface of the respective supports. Thus, the present Raman results unambiguously suggest that vanadium oxide exists in the form of a highly dispersed monomolecular layer at lower calcination temperatures, mostly in the form of a two-dimensional polymeric vanadium oxide species, in view of the V_2O_5 contents selected (close to monolayer coverage). However, at higher calcination temperatures, because of a highly feasible solid-state interaction between the dispersed vanadium oxide and the supporting cerium oxide, a highly facile cerium orthovanadate ($CeVO_4$) compound formation takes place. Further, the present results reveal that the formation of $CeVO_4$ is primarily dependent on the nature of the support and the degree of thermal treatment.

To understand the nature of interactions between the dispersed vanadium oxide and the supporting oxides, samples were subjected to XPS analysis. The electron binding energies (eV's) of O 1s, Si 2p, Ti 2p, Zr 3d, Ce 3d, and V 2p photoelectron peaks of V_2O_5/CeO_2-MO_2 samples and their corresponding XPS atomic intensity ratios (Ce/M, V/Ce, and V/M) are presented in Table 2. In general, the electron binding energy values agree well with the literature reports.[42,43] The O 1s spectra of various samples are shown in Figure 6. The O 1s peak is, in general, broad and complicated because of the nonequivalence of surface oxygen ions. As per the literature, the oxygen ion in pure CeO_2 exhibits intense peaks at 528.6, 528.8, 529.6, and 530.1 eV.[42,43,63−65] The O 1s binding energy values reported for various other oxides, namely SiO_2, TiO_2, and ZrO_2 are 532.7, 530.0, and 530.6 eV, respectively.[42,43,63,66] The O 1s spectra of the V_2O_5/CeO_2-SiO_2 sample calcined at 773−873 K show broader asymmetric peaks due to the overlapping contributions from CeO_2 and the dispersed V_2O_5 (Figure 6a). For the purpose of better understanding, the O 1s spectra of the bare CeO_2-

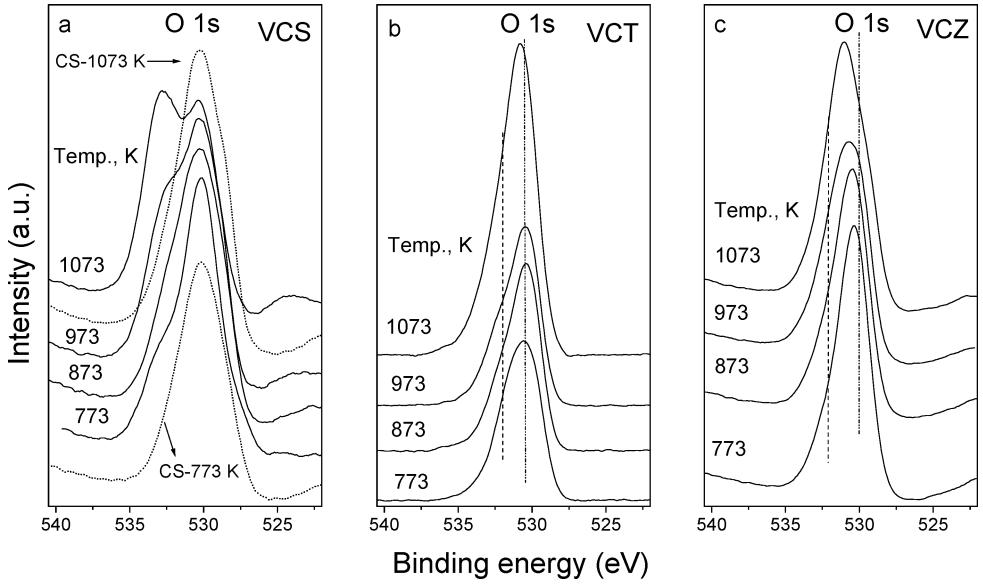

Figure 6. O 1s XPS spectra of various V_2O_5/CeO_2-MO_2 ($M = Si^{4+}$, Ti^{4+}, and Zr^{4+}) catalysts calcined at different temperatures.

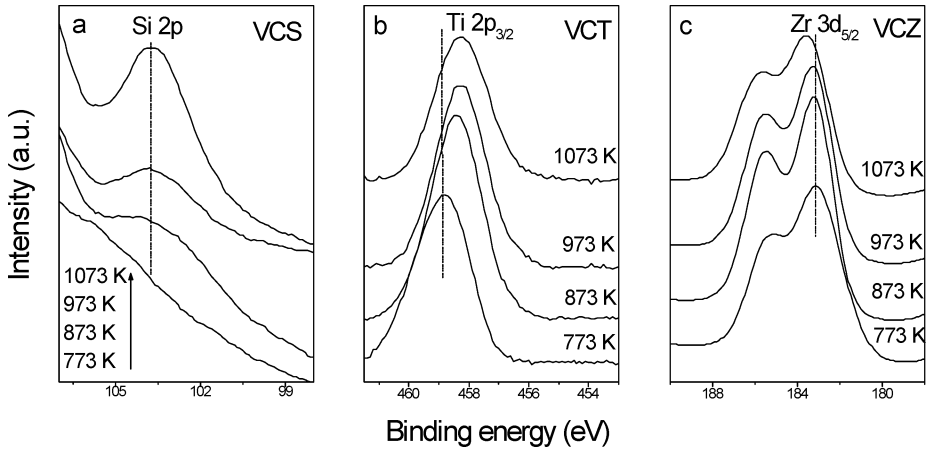

Figure 7. Si 2p, Ti 2p, and Zr 3d XPS spectra of various V_2O_5/CeO_2-MO_2 ($M = Si^{4+}$, Ti^{4+}, and Zr^{4+}) catalysts calcined at different temperatures.

TABLE 2: XPS Core-Level Binding Energies (eV) and Atomic Ratios of Various V_2O_5/CeO_2-MO_2 ($M = Si^{4+}$, Ti^{4+}, and Zr^{4+}) Samples Calcined at Different Temperatures

temp	binding energy (eV)						atomic ratio		
(K)	O 1s	Si 2p	Ti 2p	Zr 3d	Ce 3d	V 2p	Ce/M	V/Ce	V/M
			V_2O_5/CeO_2-SiO_2				M = Si		
773	530.1				881.1	517.1	0.66	0.75	0.53
873	530.2	104.0			880.9	516.8	0.62	0.77	0.48
973	530.3	103.9			880.8	516.6	0.58	0.78	0.46
1073	530.4	103.7			880.6	516.4	0.54	0.80	0.45
			V_2O_5/CeO_2-TiO_2				M = Ti		
773	530.5		458.8		881.9	517.6	2.4	0.78	1.9
873	530.4		458.5		881.7	517.4	2.1	0.77	1.6
973	530.4		458.3		881.5	517.3	1.8	0.76	1.4
1073	530.8		458.3		882.2	517.2	1.6	0.75	1.2
			V_2O_5/CeO_2-ZrO_2				M = Zr		
773	530.3			183.1	881.4	517.6	2.99	0.95	3.73
873	530.5			183.2	880.2	517.2	2.49	0.94	2.63
973	530.6			183.3	880.2	517.2	2.08	0.92	2.07
1073	531.0			183.6	880.2	517.3	1.83	0.90	1.85

SiO_2 support calcined at 773 and 1073 K are also shown in Figure 6a. With increasing calcination temperature, bifurcation of the O 1s peak is observed in the case of V_2O_5/CeO_2-SiO_2 samples, giving rise to a new peak at 532.9 eV, which can be unambiguously attributed to the formation of $CeVO_4$, in line with XRD and RS results.[45] The O 1s peak shape of the V_2O_5/CeO_2-TiO_2 sample suggests that it is composed of more than one peak arising from the overlapping contributions from ceria, titania, and dispersed vanadia. The broad peak (indicated by a dotted line) on the higher binding energy end can be attributed to the formation of the $CeVO_4$ compound, usually observed at around 532.9 eV. The O 1s profile in the case of the V_2O_5/CeO_2-ZrO_2 sample is also broad because of the overlapping contributions from Ce−Zr solid solutions, dispersed vanadia, and $CeVO_4$. The binding energy of the O 1s peak (Table 2) is found to increase with increasing calcination temperature. This shift to higher binding energy and broadening are mainly due to the formation of various Ce−Zr solid solutions in cubic and tetragonal symmetries, as well as $CeVO_4$ (shown with a dotted line), as noted from XRD and RS studies.

Figure 7a shows the Si 2p photoelectron peaks of the V_2O_5/CeO_2-SiO_2 sample calcined at different temperatures. The binding energy of the Si 2p peak ranged between 103.6 and 104.0 eV, which agrees well with the values reported in the literature.[42,43] However, the spectra are very broad with less intensity, indicating that the silica surface is not easily accessible at the surface because of the presence of ceria and the dispersed vanadium oxide overlayers. However, an increase in the intensity of the peak can be seen at higher calcination temperatures. This is mainly due to the redistribution of various components in the V_2O_5/CeO_2-SiO_2 sample under the influence of high-temperature calcination. The strong interaction between the

dispersed vanadium oxide and the ceria to form a stable $CeVO_4$ compound is associated with a progressive exposure of the SiO_2 surface, as observed with the appearance of the Si 2p peak at 103.7 eV. The Ti 2p photoemission spectra of the V_2O_5/CeO_2-TiO_2 sample calcined at different temperatures exhibit (Figure 7b) typical XPS peaks in the range 458.8−458.3 eV, which agree well with the values reported in the literature for stoichiometric TiO_2 surfaces.[42,43] Hence, it can be can inferred from XPS results that titanium is mostly confined to its highest oxidation state (IV). The shift in the peak maxima toward lower binding energy with increasing calcination temperature signifies the interaction of TiO_2 with CeO_2. However, no definite compounds between them were observed from XRD and Raman studies. As shown in Figure 7c and Table 2, the binding energy of the Zr 3d photoelectron peak pertaining to V_2O_5/CeO_2-ZrO_2 samples ranged between 182 and 182.4 eV, which agrees well with the values reported in the literature for $Zr(IV)O_2$.[42,43] The Zr 3d core-level spectra show a progressive broadening, along with a shift toward higher binding energy, indicating the formation of solid solutions between ceria and zirconia in different stoichiometric combinations with increasing calcination temperature, in conformity with XRD observations. The shift also signifies the zirconia enrichment of the surface and accounts for the emergence of zirconia-rich composite oxides at higher calcination temperatures.[42,43]

The XPS core-level spectra of Ce 3d are generally characterized by complex but distinct features that are related to the final-state occupation of the Ce 4f level.[65] In general, the assignment of CeO_2 3d photoelectron peaks is ambiguous because of the complex nature of the spectra, arising not only because of the multiple oxidation states but also from mixing of Ce 4f levels and O 2p states during the primary photoemission process. This hybridization leads to splitting of the peaks into doublets, with each doublet showing further structure due to final-state effects.[65] On the whole, the Ce 3d spectra of the V_2O_5/CeO_2-SiO_2 and V_2O_5/CeO_2-ZrO_2 samples calcined at 773 K essentially signified the presence of the Ce^{4+} oxidation state. However, the V_2O_5/CeO_2-TiO_2 sample exhibited a myriad of peaks indicating the presence of Ce^{3+}/Ce^{4+} oxidation states, on account of the partially oxidized surface.[64] With increasing calcination temperature, the relative intensities of the peaks pertaining to Ce^{3+} increased exponentially at the expense of the Ce^{4+} peaks in all of the investigated samples.[64] This observation revealed the stabilization of the Ce^{3+} oxidation state at higher calcination temperatures due to the formation of the $CeVO_4$ compound. Corresponding evidence has already been noted from XRD and RS measurements.

The V $2p_{3/2}$ photoelectron peaks of the V_2O_5/CeO_2-MO_2 ($M = Si^{4+}$, Ti^{4+}, and Zr^{4+}) samples calcined at different temperatures were, in general, broad, and their intensity increased with increasing calcination temperature. As envisaged in the literature, broadening of the XPS peaks can occur from various factors including (1) the presence of more than one type of V^{5+} species with different chemical characteristics, which cannot be discerned by ESCA, and (2) electron transfer between the active component and the support (metal oxide−support oxide interaction).[5,37,67,68] As per the literature, the binding energy of V $2p_{3/2}$ reported for V_2O_5 (V^{5+} oxidation state) ranges between 517.4 and 516.4 eV; the next oxidation state, V^{4+}, represented by V_2O_4, shows values in the range 515.7−515.4 eV.[67,68] As presented in Table 2, there is a slight decrease in the V 2p binding energy with increasing calcination temperature for all samples, which is an indication of some reduction of the V oxide species at the surface under the influence of high-temperature treatment. However, most of the vanadium is in the V^{5+} oxidation state due to the formation of $CeVO_4$ compound. Thus, the XPS measurements support the conclusions drawn from XRD and RS results.

The relative dispersion of vanadium oxide on the support surface was estimated from XPS atomic-intensity-ratio measurements. The V/Ce and V/M ($M = Si^{4+}$, Ti^{4+}, and Zr^{4+}) atomic ratios can be taken as a measure of relative dispersion of vanadium oxide on the mixed-oxide surface. The Ce/M, V/Ce, and V/M (M = Si, Ti, and Zr) atomic ratios as determined by XPS are presented in Table 2. The Ce/Si atomic ratio in the case of the V_2O_5/CeO_2-SiO_2 samples decreased with increasing calcination temperature. Redistribution of dispersed vanadia and ceria under the influence of thermal treatments facilitates the progressive release of silica surface, which was covered by these oxide overlayers. The exposure of SiO_2 surface increases the Si 2p peak intensity and thereby accounts for the decrease in Ce/Si atomic ratios. The V/Ce ratio was found to increase with increasing calcination temperature, whereas the V/Si ratio decreased. It is quite obvious that most of the dispersed vanadium oxide is confined to the ceria by forming $CeVO_4$, as vanadia and silica interactions are very weak.[5] Upon the increase of calcination temperature, the so-formed $CeVO_4$ agglomerates into bigger particles, thereby leaving part of the silica surface uncovered. Thus, the atomic intensity variations can be explained by the formation of $CeVO_4$ and the crystallization of the remaining CeO_2 under the influence of high-temperature calcinations. As can be observed from Table 2, the Ce/Ti atomic ratios, in the case of V_2O_5/CeO_2-TiO_2 samples, decrease as a function of increasing calcination temperature. Here again, the redistribution of various component oxides due to the formation of $CeVO_4$ leads to the partial surface enrichment of TiO_2, both of which are responsible for the observed decrease in Ce/Ti, V/Ce, and V/Ti atomic ratios as a function of increasing calcination temperature. In the case of the V_2O_5/CeO_2-ZrO_2 catalyst, the observed decrease in the Ce/Zr atomic ratio with increasing calcination temperature could be attributed to the surface enrichment of zirconia due to the formation of zirconia-rich cubic and tetragonal phases over the surface. The XRD results clearly established the role of dispersed vanadium oxide in accelerating the crystallite growth and tetragonalization of the Ce−Zr solid solutions. As can be noted from Table 2, the V/Ce and V/Zr ratios are also found to decrease with increasing calcination temperature. The slight decrease in V/Ce ratio could be due to the surface segregation of vanadia and ceria species caused by the formation of the $CeVO_4$ compound at higher calcination temperatures. The incorporation of zirconia into the ceria lattice and formation of the tetragonal $Ce_{0.16}Zr_{0.84}O_2$ phase might be responsible for a greater decrease in the V/Zr atomic ratios.

The preferential formation of the $CeVO_4$ compound at higher calcination temperatures, due to solid-state reactions between the dispersed vanadium oxide and the ceria portion of the CeO_2-MO_2 ($M = Si^{4+}$, Ti^{4+}, and Zr^{4+}) mixed oxides, seems to be an interesting observation in this study. The $CeVO_4$ has been reported to be the catalytically active phase for various reactions.[28,29,32] The formation of the $CeVO_4$ phase can be explained by taking into account the charge-to-radius ratio of the mixed oxides as envisaged by Bond et al.[5] The formation of surface compounds or unidimensional layers of vanadium oxide on various oxide supports has been related to the ratio of the charge of the support cation to the sum of the radii of cation and oxide ions (q/r).[5] Normally, lower q/r ratios favor surface compound formation. The q/r ratio for the vanadia−ceria

combination is lower, because the radius of Ce^{4+} (0.97 Å) is higher than any of the constituent oxide ions Si^{4+} (0.41 Å), Ti^{4+} (0.64 Å), or Zr^{4+} (0.84 Å). Therefore, the dispersed vanadium oxide is expected to interact selectively with the ceria portion of the mixed oxide, thereby leading to the formation of the $CeVO_4$ crystalline surface compound. The PZC (point of zero charge or pH at surface neutrality) values reported in the literature also support these observations.[5,50,59] The PZC of ceria (8.1 ± 0.1) is much higher than that of silica (3.9 ± 0.1), titania (5.9 ± 0.1), or zirconia (5.9−6.1), thus making it more basic. The PZC of vanadia falls into the high acidic pH range (0.5). Therefore, a highly facile acid−base interaction is expected between the dispersed vanadium oxide and the ceria, leading to the formation of the $CeVO_4$ compound.

4. Conclusions

1. The dispersion and surface structure of V_2O_5 on CeO_2-MO_2 ($M = Si^{4+}$, Ti^{4+}, and Zr^{4+}) mixed-oxide supports were the main focus of this investigation. The techniques of XRD, RS, XPS, and BET surface area were employed to study these systems. The investigated 1:1 mole ratio of CeO_2-MO_2 mixed oxides was prepared by soft chemical methods with ultrahigh-dilution solutions. These procedures yield fairly homogeneous and stable mixed oxides with reasonably high specific surface areas. The XRD and RS results revealed that the CeO_2-MO_2 carrier (calcined at 773 K) exhibits the presence of nanocrystalline cubic CeO_2 on the surface of SiO_2 in CeO_2-SiO_2, CeO_2 and TiO_2 (anatase) in CeO_2-TiO_2, and $Ce_{0.75}Zr_{0.25}O_2$ in CeO_2-ZrO_2 samples.

2. A nominal monolayer equivalent of V_2O_5 was impregnated over the mixed-oxide supports, and the obtained catalysts were subjected to calcination at different temperatures from 773 to 1073 K. The XRD and RS results suggested that vanadium oxide is present in a highly dispersed amorphous state on all of the supports when calcined at 773 K. However, the impregnated vanadia over CeO_2-MO_2 induces various modifications when subjected to high calcination temperatures.

3. The dispersed vanadia on the CeO_2-MO_2 carrier induces better crystallization of various phases and interacts selectively with CeO_2 to form $CeVO_4$ in all samples. The $CeVO_4$ formation was noted at 773, 873, and 973 K in CeO_2-TiO_2, CeO_2-SiO_2, and CeO_2-ZrO_2 samples, respectively.

4. In the case of CeO_2-ZrO_2 samples, the incorporation of more zirconia into the cubic $Ce_{0.75}Zr_{0.25}O_2$ lattice occurred, leading to the formation of the tetragonal $Ce_{0.16}Zr_{0.84}O_2$ phase at higher calcination temperatures.

5. The RS results, in particular, provided evidence for the presence of oxygen vacancies/Ce^{3+} in all samples in different proportions.

6. The XPS measurements indicated that O 1s, Ce 3d, Si 2p, Ti 2p, and Zr 3d core-level photoelectron peaks are sensitive to the dispersed vanadium oxide and the calcination temperature.

Acknowledgment. P.L. and A.K. thank CSIR, New Delhi, for a Junior Research Fellowship and DST, New Delhi, for a Research Fellowship under SERC scheme (SP/S1/H-20/98), respectively. Authors thank Dr. S. Loridant, IRC-Lyon, France, and Dr. Y. Yamada, AIST-Osaka, Japan, for providing Raman and XPS results, respectively.

References and Notes

(1) Hirao, T. *Chem. Rev.* **1997**, *97*, 2707.
(2) Bañares, M. A., Wachs, I. E., Eds. *Catal. Today* **2003**, *78*, 1−582 (special issue).
(3) Reddy, B. M. Redox Properties of Metal Oxides. In *Metal Oxides: Chemistry and Applications*; Fierro, J. L. G., Ed., Marcel Dekker, in press.
(4) Védrine, J. C., Ed. Eurocat Oxide. *Catal. Today* **1994**, *20*, 1.
(5) Bond, G. C.; Tahir, S. F. *Appl. Catal.* **1991**, *71*, 1; and references therein.
(6) Chen, K.; Khodakov, A.; Yang, J.; Bell, A. T.; Iglesia, E. *J. Catal.* **1999**, *186*, 325.
(7) Concepción, P.; López-Nieto, J. M.; Pérez-Pariente, J. *J. Mol. Catal. A: Chem.* **1995**, *99*, 173.
(8) Bosch, H.; Janssen, F. *Catal. Today* **1988**, *2*, 369.
(9) Amiridis, M. D.; Wachs, I. E.; Deo, G.; Jehng, J, M.; Kim, D. S. *J. Catal*. **1996**, *161*, 247.
(10) Nikolov, V.; Klissurski, D.; Anastasov, A. *Catal. Rev.—Sci. Eng*. **1991**, *33*, 1.
(11) Reddy, B. M.; Kumar, M. V.; Ratnam, K. J. *Appl. Catal., A* **1999**, *181*, 77.
(12) Cavelli, P.; Cavani, I.; Manenti, I.; Trifiro, F. *Catal. Today* **1987**, *1*, 245.
(13) Reddy, B. M.; Manohar, B. *Chem. Ind. (London)* **1992**, 182.
(14) Weckhuysen, B. M.; Wang, D.; Rosynek, M. P.; Lunsford, J. H. *J. Catal.* **1998**, *175*, 347.
(15) Trovarelli, A. *Catalysis by Ceria and Related Materials*; Catalytic Science Series; World Scientific Publishing Company: London, 2002; Vol. 2.
(16) Bernal, S., Kasper, J., Trovarelli, A., Eds. Recent Progress in Catalysis by Ceria and Related Compounds. *Catal. Today* **1999**, *50*, 173.
(17) Kaspar, J.; Fornasiero, P.; Graziani, M. *Catal. Today* **1999**, *50*, 285.
(18) Sahibzada, M.; Steele, B. C. H.; Zheng, K.; Rudkin, R. A.; Metcalfe, I. S. *Catal. Today* **1997**, *38*, 459.
(19) Larachi, F.; Pierre, J.; Adnot, A.; Bernis, A. *Appl. Surf. Sci*. **2002**, *195*, 236.
(20) Qi, G.; Yang, R. T. *J. Chem. Soc., Chem. Commun*. **2003**, 848.
(21) Trovarelli, A.; de Leitenburg, C.; Boaro, M.; Dolcetti, G. *Catal. Today* **1999**, *50*, 353.
(22) Zamar, F.; Trovarelli, A.; de Leitenburg, C.; Dolcetti, G. *J. Chem. Soc., Chem. Commun.* **1995**, 965.
(23) Centeno, M. A.; Paulis, M.; Montes, M.; Odriozola, J. A. *Appl. Catal., A* **2002**, *234*, 65.
(24) Trovarelli, A.; de Leitenburg, C.; Dolcetti, G. *CHEMTECH* **1997**, *27*, 32.
(25) Bernal, S.; Calvino, J. J.; Cauqui, M. A.; Gatica, J. M.; Larese, C.; Pérez-Omil, J. A.; Pintado, J. M. *Catal. Today* **1999**, *50*, 175.
(26) Nagai, Y.; Yamamoto, T.; Tanaka, T.; Yoshida, S.; Nonaka, T.; Okamoto, T.; Suda, A.; Sugiura, M. *Catal. Today* **2002**, *74*, 225.
(27) Sugiura, M. *Catal. Surv. Jpn.* **2003**, *7*, 77.
(28) Daniell, W.; Ponchel, A.; Kuba, S.; Anderle, F.; Weingand, T.; Gregory, D. H.; Knözinger, H. *Top. Catal*. **2002**, *20*, 65.
(29) Rane, V. H.; Rajput, A. M.; Karkamkar, A. J.; Choudhary, V. R. *Appl. Energy* **2004**, *77*, 375.
(30) Feng, T.; Vohs, J. M. *J. Catal.* **2004**, *221*, 619.
(31) Burcham, L. J.; Deo, G.; Gao, X.; Wachs, I. E. *Top. Catal.* **2000**, *11/12*, 85.
(32) Li, K. T.; Chi, Z. H. *Appl. Catal., A* **2001**, *206*, 197.
(33) Wootsch, A.; Descorme, C.; Duprez, D. *J. Catal*. **2004**, *225*, 259.
(34) Usmen, R. K.; Graham, G. W.; Watkins, W. L. H.; McCabe, R. W. *Catal. Lett.* **1995**, *30*, 53.
(35) Cho, B. K. *J. Catal.* **1991**, *131*, 74.
(36) Reddy, B. M.; Ganesh, I.; Chowdhury, B. *Catal. Today* **1999**, *49*, 115.
(37) Deo, G.; Wachs, I. E.; Haber, J. *Crit. Rev. Surf. Chem.* **1994**, *4*, 141.
(38) Concepción, P.; Reddy, B. M.; Knözinger, H. *Phys. Chem. Chem. Phys.* **1999**, *1*, 3031.
(39) Baiker, A.; Dollenmeier, P.; Glinski, M.; Reller, A. *Appl. Catal.* **1997**, *35*, 351.
(40) Reddy, B. M.; Ganesh, I.; Reddy, E. P.; Fernandez, A.; Smirniotis, P. G. *J. Phys. Chem. B* **2001**, *105*, 6227.
(41) Klug, H. P.; Alexander, L. E. *X-ray Diffraction Procedures for Polycrystalline and Amorphous Materials*, 2nd ed.; John Wiley and Sons: New York, 1974.
(42) Auger and X−ray Photoelectron Spectroscopy. *Practical Surface Analysis*, 2nd ed.; Briggs, D., Seah, M. P., Eds; Wiley: New York, 1990; Vol. 1.
(43) Wagner, C. D.; Riggs, W. M.; Davis, L. E.; Moulder, J. F. In *Handbook of X-ray Photoelectron Spectroscopy*; Muilenberg, G. E., Ed., Perkin-Elmer Corporation: Eden Prairie, MN, 1978.
(44) Reddy, B. M.; Khan, A.; Yamada, Y.; Kobayashi, T.; Loridant, S.; Volta, J. C. *J. Phys. Chem. B* **2003**, *107*, 11475.
(45) Reddy, B. M.; Khan, A.; Yamada, Y.; Kobayashi, T.; Loridant, S.; Volta, J. C. *J. Phys. Chem. B* **2002**, *106*, 10964.
(46) Rocchini, E.; Trovarelli, A.; Llorca, J.; Graham, G. W.; Weber, W. H.; Maciejewski, M.; Baiker, A. *J. Catal.* **2000**, *194*, 461.

(47) Rocchini, E.; Vicario, M.; Llorca, J.; de Leitenburg, C.; Dolcetti, G.; Trovarelli, A. *J. Catal.* **2002**, *211*, 407.
(48) Preuss, A.; Gruehn, R. *J. Solid State Chem.* **1994**, *110*, 363.
(49) Reddy, B. M.; Khan, A.; Yamada, Y.; Kobayashi, T.; Loridant, S.; Volta, J. C. *Langmuir* **2003**, *19*, 3025.
(50) Bañares, M. A.; Wachs, I. E. *J. Raman Spectrosc.* **2002**, *33*, 359.
(51) Martinez-Arias, A.; Fernandez-Garcia, M.; Salamanca, L. N.; Valenzuela, R. X.; Conesa, J. C.; Soria, J. *J. Phys. Chem. B* **2000**, *104*, 4038.
(52) Shyu, J. Z.; Weber, W. H.; Gandhi, H. S. *J. Phys. Chem.* **1988**, *92*, 4964.
(53) Lin, X.-M.; Li, L.-P.; Li, G.-S.; Su, W.-H. *Mater. Chem. Phys*. **2001**, *69*, 236.
(54) Spanier, J. E.; Robinson, R. D.; Zhang, F.; Chan, S.-W.; Herman, I. P. *Phys. Rev. B* **2001**, *64*, 245407.
(55) Weber, W. H.; Hass, K. C.; McBride, J. R. *Phys. Rev. B* **1993**, *48*, 178.
(56) McBride, J. R.; Hass, K. C.; Poindexter, B. D.; Weber, W. H. *J. Appl. Phys*. 1**994**, *76*, 2435.
(57) Wachs, I. E.; Deo, G. *J. Phys. Chem*. **1991**, *95*, 5889.
(58) Jehng, J. M. *J. Phys. Chem. B* **1998**, *102*, 5816.
(59) Kosmulski, M. *Adv. Colloid Interface Sci.* **2002**, *99*, 255.
(60) Griffith, W. P.; Lesniak, P. J. B. *J. Chem. Soc. A* **1969**, 1066.
(61) Knözinger, H.; Mestl, G. *Top. Catal*. **1999**, *8*, 45.
(62) Olthof, B.; Khodakov, A.; Bell, A. T.; Iglesia, E. *J. Phys. Chem. B* **2000**, *104*, 1516.
(63) Bensalem, A.; Bozon-Verduraz, F.; Delamar, M.; Bugli, G. *Appl. Catal., A* **1995**, *121*, 81.
(64) Fierro, J. L. G.; Soria, J.; Sanz, J.; Rojo, J. M. *J. Solid State Chem*. **1987**, *66*, 154.
(65) Burroughs, A.; Hamnett, A.; Orchard, A. F.; Thornton, G. *J. Chem. Soc., Dalton Trans*. **1976**, *1*, 1686.
(66) Biener, J.; Baumer, M.; Wang, J.; Madrix, R. J. *Surf. Sci*. **2000**, *450*, 12.
(67) Bukhtiyarov, V. I. *Catal. Today* **2000**, *56*, 403.
(68) Nag, N. K.; Massoth, F. E. *J. Catal*. **1990**, *124*, 127.